DOI 10.4430/bgo00394

Investigation of ionospheric TEC changes potentially related to Seferihisar-Izmir earthquake (30 October 2020, M_w 6.6)

F. Basciftci[1] and S. Bulbul[2]

[1] *Vocational School of Technical Science, Karamanoğlu Mehmetbey University, Karaman, Turkey*
[2] *Department of Geomatic Engineering, Faculty of Engineering and Natural Sciences, Konya Technical University, Konya, Turkey*

(Received: 18 May 2021; accepted: 29 April 2022; published online: 27 July 2022)

ABSTRACT It is important to be able to predict the occurrence time of an earthquake in order to take measures against its destructive effects. One of the parameters to be considered in earthquake prediction is ionospheric changes. Numerous studies have shown some changes in the ionosphere layer before or after the earthquake. These changes can be modelled to be detected with different methods and devices. One of the main parameters in examining these methods is the change of the Total Electron Content (TEC). With Global Navigation Satellite Systems (GNSS) observations, the TEC changes in the ionosphere can be determined before, during and after the earthquake. In this study, the changes in the ionosphere caused by the Seferihisar-Izmir earthquake (37.8881° N 26.7770° E, 30 October 2020, M_w 6.6) were investigated in a 58-day time interval, including pre-earthquake, earthquake day, and post-earthquake. Firstly, the indices of solar activity (F10.7), Geomagnetic Activity (Dst), and Geomagnetic Storm (Kp) that can affect the ionosphere change pre-earthquake, earthquake day, and post-earthquake were examined. Then, the effects of the earthquake on the TEC changes in the ionosphere were investigated with the TEC values obtained from the regional ionospheric TEC (RIM-TEC), obtained from GNSS receivers in the earthquake zone and its surroundings, and global TEC maps (CODE). The indices showed that there were no geomagnetic activities between 29 September and 25 November 2020. In the study carried out, it was concluded that it is more accurate to calculate TEC values regionally rather than from Global TEC maps in the case of major episodic effects such as earthquakes. In addition, in the results about the TEC anomaly, it would seem that there was a maximum anomaly 8 days before the 304th day of 2020.

Key words: GNSS, ionosphere, Seferihisar-Izmir earthquake, space weather conditions, TEC.

1. Introduction

The Earth's atmosphere is divided into five main layers according to temperature and is protected by gravity. The layers, from the nearest to the Earth's surface to the highest above it, are the troposphere, stratosphere, mesosphere, thermosphere, and exosphere, respectively. The ionosphere is the ionised part of the upper atmosphere, ranging from 60 to 1000 km, and contains the entire thermosphere and mesosphere, and some parts of the exosphere (Alcay and Gungor, 2020).

Most of the ionosphere consists of neutral gases. Ionised gases are mostly formed as a result of ionisation by short-wave (ultraviolet and X-radiation) rays from the Sun. The amount of free electrons in the ionosphere depends on many factors such as time, location, and geomagnetic mobility (Basciftci *et al.*, 2017). The ionosphere exhibits some regular, temporal, and regional changes, such as daily, 27-day, seasonal, 6-month, annual, and 11-year changes. These changes can be modelled and their impact largely determined. In addition to regular changes, unexpected irregular changes in the ionosphere (Sentürk and Cepni, 2018; Alcay and Gungor, 2020) are caused by many factors such as space weather conditions (solar flares, geomagnetic storms, etc.), geological natural hazards (earthquakes, volcanic explosions, etc.), and human-induced events (rocket launches, nuclear explosions, etc.).

It is important to be able to predict the occurrence time of an earthquake in order to take measures against its destructive effects. The effects of the crustal movements that occur on the Earth not only take the form of shaking, but also cause changes that human beings cannot perceive directly. These changes can be modelled so that they can be detected with different methods and devices. One of the main parameters in the examination of these methods is the change of the Total Electron Content (TEC) value (Ulukavak and Yalcinkaya, 2014). TEC, which is the most important function of the ionosphere layer and expresses the total amount of free electrons, is defined as the total number of electrons in a 1 m^2 base cylinder. Its unit is TECU and 1 TECU is accepted as approximately 10^{16} electrons/m^2 (Wild, 1994; Schaer, 1999; Ya'acob *et al.*, 2010). The total amount of electrons is a function of solar, geomagnetic, gravitational, atmospheric, electrical, and seismic changes. Global Navigation Satellite System (GNSS) technology provides low cost, high accuracy, near real-time, continuous ionospheric data. While determining the TEC, it is necessary to investigate the geomagnetic effects, which have a significant disruptive effect on the GNSS measurements, and to separate geomagnetic effects from the effects of the earthquake in the GNSS measurements.

Geomagnetic effects are associated with irregular effects occurring in the ionosphere layer (Nishino *et al.*, 1998; Skone and Cannon, 1999; Aquino *et al.*, 2001; Ping *et al.*, 2002; Arslan, 2004). The effects that cause irregular changes in the ionosphere layer are especially due to solar-induced magnetic activities (Arslan, 2004; Alcay and Gungor, 2020).

The ionosphere causes GPS signal delays to be proportional to TEC along the path from the GPS satellite to a receiver (Hofmann-Wellenhof *et al.*, 2008). The ionospheric delay is proportional to the number of electron content and inversely proportional to the frequency squared (Bhattacharya *et al.*, 2008). The Sun plays a vital role in the magnitude of this error, because high levels of solar activity that increase the amount of refraction induced by the ionosphere (Sickle, 2015). The solar wind is a stream of charged particles released from the upper atmosphere of the Sun. The solar wind reacts with the geomagnetic field, and occasionally, these charged particles rise significantly due to the solar flares on the surface of the Sun (Klobuchar, 1991). Coronal Mass Ejections (CMEs) are large expulsions of plasma and magnetic field from the Sun's corona. The CMEs hitting our planet will significantly distort the Earth's magnetic field and induce geomagnetic storms (Sidorov *et al.*, 2019; Sedeek, 2020). The effects of geomagnetic storms can spread to mid and low (equatorial) latitudes as well as high latitudes. Such storms disrupt the ionosphere and degrade the performance of the GPS receiver (Elsayed *et al.*, 2018; Elghazouly *et al.*, 2019; Sedeek, 2020). As the Earth's magnetic field changes for this reason, the ruptured particles also affect the Earth's neutral atmosphere, generating additional electrons and creating a strong electric field. These events create changes in the ionosphere (Parkinson and Spilker, 1996; Arslan, 2004). The generated electric field shows itself as progress in phase observations in a time like one minute and a delay in code observations. The time of change may

vary by region. For example, in the polar regions, this change can take several hours. For GPS receivers, this effect can cause difficulties in receiving signals as well as preventing them from receiving signals (Teunissen and Kleusberg, 1998; Arslan, 2004).

Kp index, Disturbance storm time (Dst) index, Solar Flux values are indicators of magnetic activity and, therefore, changes in the ionosphere. Kp index, Dst index and events such as solar flare may be relevant in the analysis of GNSS data. Solar flares are events involving energy releases spanning from radio waves to gamma rays. They may produce streams of highly energetic particles in the solar wind. Such particles can impact the Earth's magnetosphere (Stewart and Langley, 1998; Jakowski *et al.*, 2001; Arslan, 2004).

The Kp index is a geomagnetic storm index that determines the magnetic effects of the planet and may be used to show the effects of the solar wind on the Earth's magnetic field. The Kp index was introduced by Bartels (1938). The Kp index is derived by calculating a weighted average of K indices from a network of 13 geomagnetic observatories at mid-latitude locations. Since these observatories do not report their data in real-time, various operations centres around the globe estimate the index based on data available from their local network of observatories (Bartels *et al.*, 1939; Fleming *et al.*, 1939). The 3-hourly ap (equivalent range) index is derived from the Kp index (https://www.ngdc.noaa.gov/stp/GEOMAG/kp_ap.html). It is derived at 3-hour intervals using Earth-based magnetometers worldwide.

The Dst index is an index of magnetic activity derived from a network of near-equatorial geomagnetic observatories that measures the intensity of the globally symmetrical equatorial electrojet. The Dst index is obtained at 1-hour intervals using low latitude magnetograms from 4 observation stations (Mosna *et al.*, 2007; Zolesi and Cander, 2014). Also, the index refers to the decrease of the component of the magnetic field in the horizontal plane at the equator (http://wdc.kugi.kyoto-u.ac.jp/index.html; http://isgi.unistra.fr/indices_dst.php). A Dst index of -30 or deeper indicates a storm-level geomagnetic disturbance. The Dst unit is nanoTesla (nT) (Hunsucker and Hargreaves, 2003; Sharma *et al.*, 2010). Magnetic storm degrees of Kp and Dst are shown in Table 1.

Table 1 - Magnetic storm degrees of Kp (URL 1) and Dst indices (Loewe and Prölss, 1997).

Magnetic storm degrees	Kp index	Dst index
G1 Weak	5	-30 > Dst > -50
G2 Moderate	6	-50 > Dst > -100
G3 Strong (intense)	7	-100 > Dst > -200
G4 Severe (very intense)	8	-200 > Dst > -350
G5 Extreme	9	-350 > Dst

Solar flux criteria can be determined by using solar flux measurements by means of a wave with a wavelength of 10.7 cm in observing the changes in the ionosphere layer. Solar flux measurements with a 10.7 cm wavelength, which is a better method than determining the number of sunspots and level of ionisation, are recorded by the Dominon Radio Astrophysics Observatory operated by the Canadian Research Association (CNRC) at 20:00 daily depending on the Universal Time (UT) (Arslan, 2004). Solar flux at 10.7 cm wavelength is indeed measured in solar flux units (sfu), where 1 sfu = 10^{-22} Wm^{-2} Hz^{-1}, but sfu is used to measure solar flux at any wavelength (URL 2).

Since GNSS-based TEC data is among the main parameters that can be used, it is preferred in most studies on earthquakes. Liu *et al.* (2004) investigated 20 earthquakes larger than M_w 6 in Taiwan between 1999 and 2002. They applied the 15 day moving median and quarter range method to the TEC variation using GPS-based TEC data. The results showed that ionospheric anomalies were detected before earthquakes with an 80% success rate. Liu *et al.* (2010) reported seismo-ionospheric precursors due to abnormal decreases in the TEC variation five days before the Sumatra-Andaman earthquake of M_w 9.1 in 2004. Fuying *et al.* (2011) used the Kalman filter method to detect abnormal changes in TEC variations before and after the Wenchuan M_s 8.0 earthquake. TEC data were calculated from GPS observations observed by the China Crustal Motion Observation Network (CMONOC). The result showed that the Kalman filter is plausible and reliable in detecting TEC anomalies associated with major earthquakes. Karia *et al.* (2014) report the modification in GPS-TEC and atmospheric refractivity prior to the Iran earthquake of 16 April 2013. The result was that the atmospheric refraction changed from 6 to 8 days before the earthquake, and there were changes in GPS-TEC a few days before the earthquake. While searching for precursor signs for an earthquake, they concluded that both GPS-TEC and refraction are important parameters. Zhu *et al.* (2014) conducted a new statistical study using the statistical analysis method on the temporal distribution of GPS-TEC anomalies before $M_w \geq 7.0$ magnitude earthquakes between 2003 and 2012. The temporal distribution of ionospheric TEC anomalies before $M_w \geq 7.0$ earthquakes was studied for the first time. It has been observed that ionospheric negative anomalies mainly occur one week before earthquakes and only when the magnitude is greater than or equal to 7.6, and that ionospheric anomalies will have the highest probability until sunset in the afternoon. The relationship between the rate of occurrence of ionospheric anomalies before an earthquake and the magnitude of the earthquake has been discussed, and it has been found that the ionospheric TEC anomalies observed a few days before the earthquakes are likely to be associated with earthquakes. Yildirim *et al.* (2016) investigated both TEC and positional changes separately following the earthquake of M_w 6.5 that occurred on 24 May 2014 at 12:25 local time (LT) offshore the Aegean Sea with central coordinates 40.21080° N, 25.30730° E. They used four Continuously Operating Reference Stations-Turkey (CORS-TR) and 11 IGS and EUREF stations to investigate ionospheric disturbances. It was observed that the TEC data obtained from the Precise Point Positioning (PPP-TEC), calculated with a PPP.PCF module in Bernese software using Global Ionosphere Maps (GIMs), decreased by 4-5 TECU 3 days before the earthquake and the day before the earthquake. Ulukavak and Yalcinkaya (2017) used GNSS-based TEC data from 6 IGS stations to determine pre-earthquake ionospheric anomalies for the M_w 7.2 Baja, California earthquake of 4 April 2010. The results showed that both positive and negative ionospheric anomalies occurred one to five days before the earthquake. Thomas *et al.* (2017) conducted a direct analysis of seismic activity and seismic changes in GIM-TEC by examining 1279 earthquakes with $M \geq 6.0$ between 2000 and 2014 to test the possible statistical significance of TEC changes and seismic activity. Although all 1279 earthquakes were considered together in the study, no statistically significant change was found before the earthquakes in the analysis. They concluded that the GIM-TEC analysis is unlikely to be usable to identify precursors or to predict earthquakes. Ke *et al.* (2018) used a linear model between TEC and solar activity (F10.7) to detect seismo-ionospheric TEC anomalies before and after the Nepal earthquake in 2015. The method is compared with the floating quarter and Kalman filter methods. In temporal and spatial analyses, it was concluded that the linear model is more effective in detecting TEC anomalies caused by the Nepal earthquake. Tariq *et al.* (2019) used GNSS-based TEC data to detect seismo-ionospheric anomalies of 3 major earthquakes ($M_w > 7.0$) on the Nepal and Iran-Iraq border from 2015 to 2017. The ionospheric precursors of the 3 earthquakes generally occurred

within 10 days, between approximately 08:00 and 12:00 UT. Temporal and spatial statistical tests showed that abnormally positive TEC changes were detected 9 days before the M_w 7.3 Iran-Iraq earthquake. In Sentürk *et al.* (2020), temporal, spatial, and spectral analyses were applied to GNSS-based TEC data to detect ionospheric anomalies before the M_w 7.3 Iran-Iraq border earthquake on 12 November 2017. A short-time Fourier transform (STFT) and a working median process were applied to identify anomalies in the TEC time series. Interplanetary magnetic field (IMF Bz), electric field (Ey), and plasma speed (VSW) indices, Kp, Dst, F10.7, Bz component were also analysed to show the effect of space weather indices on TEC disturbances. The results showed that the anomalies one to six days before the earthquake were caused by a moderate magnetic storm. Oikonomou *et al.* (2021) investigated possible atmospheric and ionospheric anomalies before the 3 major earthquakes (M_w > 6.6) that occurred in Mexico in 2016 and 2017. They performed a multi-technique analysis that included statistical and spectral analysis of ionospheric TEC and mapping of TEC and atmospheric chemical potential (ACP). They concluded that both large and small-scale ionospheric anomalies that occurred from several hours to a few days before seismic events may have been linked to future events, most of which are almost synchronous with atmospheric anomalies occurring on the same day. Eisenbeis and Occhipinti (2021), put forward the view that it is possible to make short-term earthquake predictions by obtaining Heki's TEC data in 2011, and they said that the 2011 Tohoku earthquake data showed an 'enhancement' of TEC 40 minutes before the event. The authors noted that this report had been criticised and that those who studied the subject suggested that the observed data were due to the decrease in TEC after the earthquake, which is called the ionospheric 'hole'. The key point, according to the authors, is choosing the reference curve to extract from the data to reveal either the hole or the enhancement. They show that the reference curve is highly sensitive to the degree of the polynomial and the selected time window. Therefore, they concluded that the alleged TEC enhancement may be an artifact that can be achieved by subjectively 'tuning' the reference curve, and they can further support this conclusion by conducting synthetic tests that show this possible artifact of the enhancement.

In this study, the possible effects of the earthquake (M_w 6.6), that occurred at 14:51 (Turkey time) offshore of Seferihisar (Izmir) in the Aegean Sea on 30 October 2020, on ionospheric changes have been investigated. For this purpose, firstly, values of Dst, F10.7, and Kp of 58 days, which may affect the ionosphere change before and after the earthquake, have been examined. Secondly, CODE-TEC values of CORS-TR stations located in the seismic region from Global TEC maps have been obtained, and Receiver Independent Exchange Format (RINEX) data obtained from the same stations have been processed with Bernese v5.2 GNSS software and the regional TEC values (RIM-TEC) have been calculated. The root mean square errors (RMSEs) have been calculated using the obtained TEC values (both CODE-TEC and RIM-TEC) and compared using F test for each station and day. Finally, TEC anomaly values have been calculated from the obtained TEC values. By evaluating the analyses obtained in the study, the results have been given.

2. Material and method

On 30 October 2020 at 14:51 local time, an earthquake (37.8881° N, 26.7770° E) occurred in the Aegean Sea between Doganbey-Izmir offshore and northern Samos Island. The magnitude of the earthquake was announced as M_w 6.6 (URL 3) by the Disaster and Emergency Management Presidency (AFAD), and M_w 6.9 (URL 4) by the Kandilli Observatory and Earthquake Research

Institute. The earthquake location map is given in Fig. 1. The depth of the earthquake was 16.54 km and it was a shallow earthquake (URL 3). The duration of the earthquake was determined as 15.68 seconds according to initial calculations. The earthquake was felt over a wide area, especially in Izmir province and its districts. The earthquake on 30 October 2020 occurred as a result of normal faulting at a shallow depth in the Eurasian tectonic plate in the Aegean Sea. The focal mechanism analyses show that the earthquake occurred on an E-W trending moderately inclined normal fault (URL 5).

Considering that the earthquake caused loss of life and property, it is of great importance to predict a possible earthquake. Therefore, in the study, the earthquake day, 31 days before, and 26 days after the earthquake day have been evaluated. Ten of CORS-TR stations were selected from the stations in the cities where the earthquake was felt. The RINEX data of the selected days have been obtained from the CORS-TR network covering the whole of Turkey. The stations are shown in Fig. 1 and Table 2. In Table 2, 'NONE' indicates the random code of the antenna. Detailed information on this can be obtained from https://geodesy.noaa.gov/ANTCAL/#.

Geomagnetic storms may have disruptive effects on GNSS measurements. Kp, Dst, ap, F10.7 are indexes indicators of disturbances in space weather. These index values on selected days are taken from URL 6 and shown in Fig. 2. In the study, Kp is multiplied by ten (Kp*10) in order to better display the Kp index. In Fig. 2, the vertical red line shows the earthquake day.

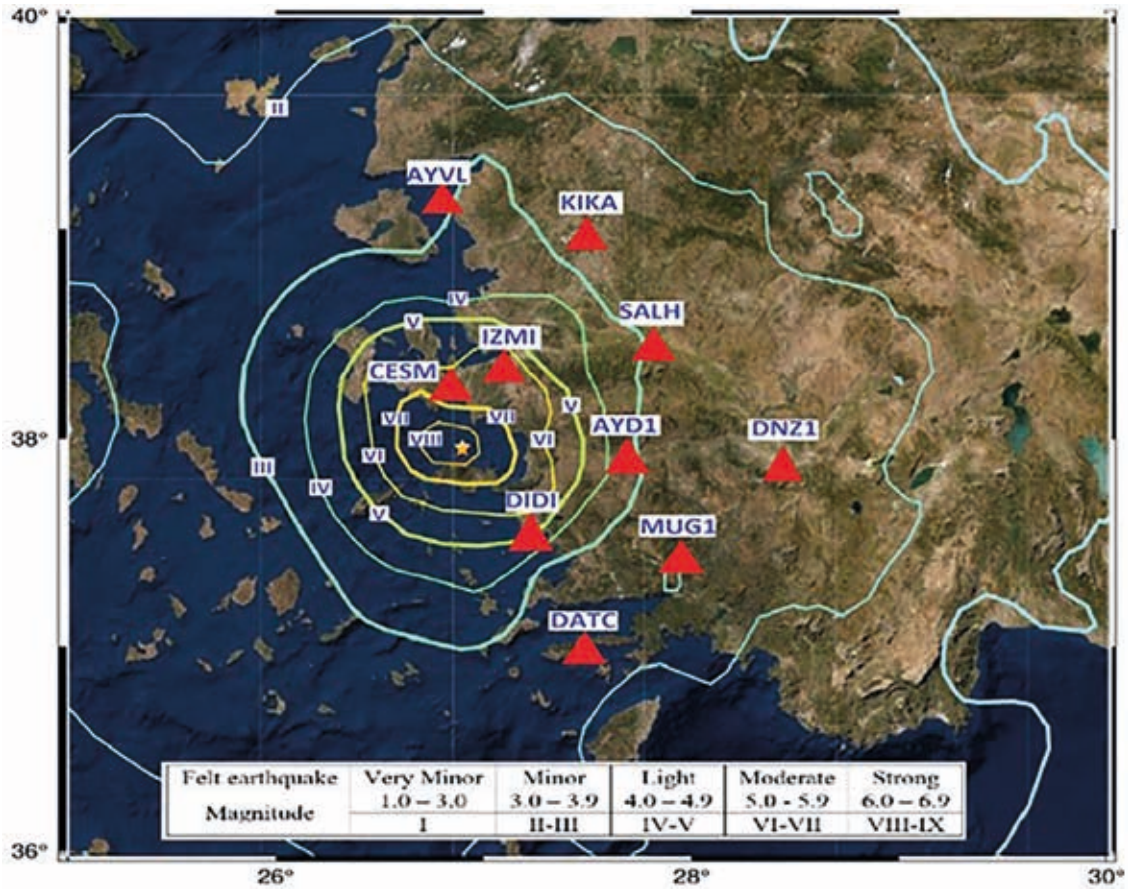

Fig. 1 - Aegean Sea earthquake location map (URL 4) and used CORS-TR stations.

Table 2 - The general information about CORS-TR stations.

PI	Lat. (° ' ") N	Long. (° ' ") E	Height (m)	Receiver	Antenna	Random
ADY1	37 45 38.08	38 15 40.45	741.18	TRIMBLE NETR5	TRM55971.00	NONE
AYVL	39 18 41.19	26 41 10.24	54.26			
CESM	38 18 13.73	26 22 21.25	52.45			
DATC	36 42 30.86	27 41 30.60	59.17			
DNZ1	37 46 43.67	29 02 37.46	537.93			
DIDI	37 22 19.66	27 16 07.17	79.27			
IZMI	38 23 41.30	27 04 54.55	74.94			
KIKA	39 06 21.56	27 40 19.94	241.21			
MUG1	37 12 51.45	28 21 20.43	693.27			
SALH	38 28 59.12	28 07 24.76	156.17			

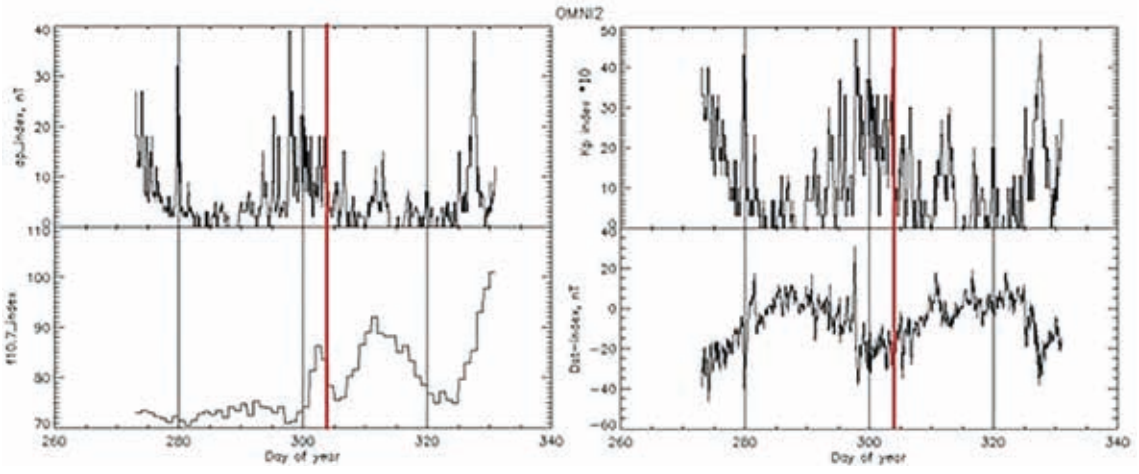

Fig. 2 - Kp, Dst, F10.7 and ap indices for 294th to 313th days of the year 2020.

When Fig 2 is examined, it is seen that Kp, Dst, and ap indices on 23-24 October 2020 (297th-298th day of year 2020) are higher than on other days, and there is no significant geomagnetic activity on the remaining days. Also, it is seen that Kp and ap indices are maximum 5 nT, 39 nT, on the 297th day of 2020, respectively. Dst index varies between -38 nT and 31 nT and F10.7 index between 71 sfu and 92.1 sfu. When Table 1 and Fig. 2 are examined together, it is seen that there is no significant activity on the selected days.

There are a lot of institutions which produce Global Ionosphere TEC maps all over the world. One of these is the Center for Orbit Determination in Europe (CODE). The Global ionosphere map (GIM) is issued in the format of IONosphere map EXchange (IONEX). IONEX formatted TEC values are lined up as occurring all over the world. The TEC at a required point may be obtained from this line. If the latitude and longitude of a point are known, the relevant TEC is obtained with the help of the four nearest TEC values covering two variable interpolation points (Schaer *et al.*, 1998). When the value calculated to determine the TEC in the TECU unit is multiplied by 0.1, the TEC value of the relevant point is determined in the TECU unit. IONEX formatted GIMs are produced at intervals of 2 hours. For TEC, the increase in the longitude is 5° and the increase in

the latitude is 2.5° (Arslan, 2004). The PPP module of Bernese v5.2 Scientific GNSS Software was used to determine the RIM-TEC changes on the selected days.

The differences (v_i) between daily average and hourly TEC values are calculated as follows:

$$v_i = TEC_{s_{d_h}} - TEC_{s_{d_{average}}}. \quad (1)$$

In Eq. 1, subscripts *s*, *d*, and *h* denote stations, day, and hour, respectively. Also, $TEC_{s_{d_{average}}}$ denotes daily average TEC for selected stations. Then, RMSE values for each day and stations are calculated as follows:

$$m_{0_d} = \pm\sqrt{\frac{[v_i v_i]}{n}}. \quad (2)$$

In Eq. 2, *n* represents the number of daily TEC values. Table 3 shows the RMSE values.

Table 3 - The daily RMSE values for RIM (TECU).

Stations	AYD1	AYVL	CESM	DATC	DIDI	DNZ1	IZMI	MUG1	KIKA	SALH
Day										
294	2.666	2.492	2.579	2.727	2.720	2.710	2.591	2.669	2.631	2.701
295	3.788	3.587	3.691	3.977	3.853	3.825	3.698	3.908	3.822	3.786
296	2.374	2.516	2.253	2.581	2.238	2.625	2.255	2.504	2.467	2.275
297	3.360	3.574	3.275	3.648	3.423	3.419	3.280	2.779	3.611	3.288
298	2.871	2.711	2.620	2.758	2.873	2.327	2.613	3.949	2.675	2.693
299	2.325	2.130	2.232	2.507	2.383	2.389	2.231	3.441	2.172	2.253
300	2.998	2.779	2.901	3.173	3.057	3.040	2.900	3.108	2.817	2.912
301	2.762	2.619	2.697	2.924	2.815	2.806	2.701	2.862	2.648	2.705
302	2.775	2.875	2.968	2.931	2.822	2.813	2.689	2.771	2.712	2.899
303	3.640	3.444	3.554	3.797	3.699	3.681	3.560	3.740	3.481	3.562
304	2.735	2.689	2.765	2.782	2.687	2.756	2.765	2.722	2.706	2.718
305	3.955	3.972	3.966	3.982	3.886	3.975	3.911	3.921	3.886	3.870
306	2.726	2.752	2.752	2.767	2.702	2.807	2.642	2.756	2.709	2.710
307	2.753	2.663	2.703	2.843	2.771	2.758	2.707	2.807	2.679	2.715
308	2.450	2.225	2.377	2.563	2.503	2.483	2.323	2.501	2.309	2.322
309	3.480	3.500	3.363	3.701	3.548	3.523	3.363	3.618	3.288	3.388
310	2.109	2.466	2.344	2.233	2.161	2.351	2.091	2.292	2.061	2.091
311	2.588	3.566	3.430	2.786	2.898	3.326	2.999	3.070	2.984	2.981
312	2.555	2.825	2.882	2.700	2.601	2.576	2.490	2.643	2.448	2.501
313	2.483	2.409	2.449	2.609	2.535	2.529	2.454	2.560	2.422	2.450

When Table 3 is examined, it is seen that the RMSE values varied between ±2.061 and ±3.977 TECU, and the highest RMSE value was obtained at the DATC station, while the minimum RMSE value was obtained at the KIKA station.

RMSE values were calculated for each station and day by using the daily TEC values published by CODE and are shown in Table 4. Table 4 shows that the RMSE values varied between ±2.645 TECU and ±4.245 TECU, and the highest RMSE value was obtained at the DATC station, while the minimum RMSE value was obtained at the AYVL station.

Table 4 - The daily RMSE values for CODE (TECU).

Stations	AYD1	AYVL	CESM	DATC	DIDI	DNZ1	IZMI	MUG1	KIKA	SALH
Day										
294	3.330	3.173	3.317	3.449	3.405	3.299	3.284	3.378	3.180	3.245
295	4.080	3.922	4.099	4.245	4.185	4.018	4.040	4.138	3.895	3.964
296	3.289	3.097	3.228	3.415	3.347	3.301	3.216	3.363	3.127	3.208
297	3.804	3.541	3.730	4.012	3.895	3.807	3.708	3.912	3.577	3.687
298	3.788	3.481	3.758	4.084	3.943	3.732	3.693	3.912	3.485	3.614
299	2.857	2.645	2.798	2.999	2.927	2.858	2.780	2.934	2.674	2.763
300	3.158	2.972	3.138	3.288	3.242	3.127	3.100	3.216	2.975	3.053
301	3.320	3.218	3.343	3.446	3.399	3.268	3.297	3.360	3.193	3.237
302	3.137	2.999	3.125	3.270	3.208	3.110	3.095	3.191	3.001	3.058
303	3.763	3.625	3.806	3.924	3.877	3.682	3.737	3.809	3.585	3.645
304	3.328	3.184	3.276	3.405	3.365	3.341	3.272	3.377	3.213	3.272
305	3.724	3.683	3.754	3.782	3.773	3.680	3.722	3.732	3.663	3.679
306	3.285	3.174	3.306	3.416	3.367	3.231	3.260	3.326	3.152	3.199
307	2.972	2.933	2.990	3.015	3.008	2.944	2.967	2.981	2.919	2.936
308	3.154	2.961	3.120	3.329	3.239	3.134	3.090	3.233	2.975	3.055
309	3.759	3.567	3.767	3.984	3.880	3.695	3.708	3.839	3.551	3.632
310	3.154	3.027	3.146	3.259	3.219	3.124	3.116	3.196	3.027	3.079
311	3.345	3.265	3.387	3.455	3.426	3.278	3.336	3.369	3.234	3.267
312	3.130	3.051	3.172	3.233	3.209	3.062	3.121	3.150	3.020	3.053
313	2.929	2.842	2.954	3.018	2.997	2.876	2.913	2.950	2.825	2.860

Because an F-test is used to determine whether the variance of two normally distributed populations are statistically equivalent, the RMSE values for each station and day are compared using an F-test.

In order to investigate whether the TEC values calculated for each day and hour at the stations are in the normal distribution, firstly, the hourly TEC values were normed with the following equation:

$$TECU_n = TECU_{dh} - TECU_{hmean} \quad (3)$$

In Eq. 3, $TECU_n$ is normed TEC value (n = 0, 2, 4, …, 22), $TECU_{dh}$ is the hourly TEC value of the selected day, $TECU_{hmean}$ shows the average of the relevant hours. Then, the class intervals were obtained from the normed TEC values and it was examined whether the hourly TEC values were in a normal distribution. In this context, the class interval of the averages of the normed TEC values of the stations and numerical information about them were given as follows.

At the AYD1 station, 10 of the 20 normalised TEC values are between -0.37 and 0.72 TECU for 0th hour, 11 of them are between -0.29 and 0.80 TECU for 2nd hour, 8 of them are between -0.13 and 1.17 TECU for 4th hour, 11 of them are between -0.68 and 0.72 TECU for 6th hour, 10 of them are between -1.08 and 0.72 TECU for 8th hour, 12 of them are between -1.54 and 0.45 TECU for 10th hour, 15 of them are between -1.54 and 1.45 TECU for 12th hour, 14 of them are between -1.65 and 1.65 TECU for 14th hour, 9 of them are between -1.38 and 0.41 TECU for 16th hour, 8 of them are between -0.33 and 0.97 TECU for 18th hour, 10 of them are between -0.80 and 0.30 TECU for 20th hour and 9 of them are between -0.39 and 0.81 TECU for 22th hour.

At the AYVL station, 10 of the 20 normalised TEC values are between -0.62 and 0.62 TECU for 0th hour, 16 of them are between -1.02 and 1.02 TECU for 2nd hour, 14 of them are between -0.54 and 0.58 TECU for 4th hour, 11 of them are between -0.77 and 0.73 TECU for 6th hour, 11 of them are between -1.17 and 0.63 TECU for 8th hour, 12 of them are between -1.60 and 0.20 TECU for 10th hour, 12 of them are between -1.05 and 0.74 TECU for 12th hour, 14 of them are between -1.12 and 1.09 TECU for 14th hour, 10 of them are between -1.30 and 0.50 TECU for 16th hour, 13 of them are between -1.01 and 1.01 TECU for 18th hour, 11 of them are between -0.55 and 0.55 TECU for 20th hour and 17 of them are between -1.09 and 1.09 TECU for 22th hour.

At the CESM station, 9 of the 20 normalised TEC values are between -0.35 and 0.75 TECU for 0th hour, 16 of them are between -0.91 and 0.91 TECU for 2nd hour, 15 of them are between -0.64 and 1.25 TECU for 4th hour, 11 of them are between -0.75 and 0.65 TECU for 6th hour, 10 of them are between -1.08 and 0.72 TECU for 8th hour, 12 of them are between -1.61 and 0.29 TECU for 10th hour, 13 of them are between -0.97 and 1.48 TECU for 12th hour, 15 of them are between -1.10 and 1.64 TECU for 14th hour, 16 of them are between -1.45 and 2.15 TECU for 16th hour, 12 of them are between -0.98 and 0.96 TECU for 18th hour, 11 of them are between -0.71 and 0.39 TECU for 20th hour and 9 of them are between -1.36 and 0.84 TECU for 22th hour.

At the DATC station, 8 of the 20 normalised TEC values are between -0.56 and 0.44 TECU for 0th hour, 10 of them are between -0.46 and 0.54 TECU for 2nd hour, 10 of them are between -0.17 and 1.13 TECU for 4th hour, 11 of them are between -0.68 and 0.72 TECU for 6th hour, 9 of them are between -1.00 and 0.80 TECU for 8th hour, 13 of them are between -1.55 and 0.55 TECU for 10th hour, 15 of them are between -1.38 and 1.51 TECU for 12th hour, 14 of them are between -1.29 and 1.36 TECU for 14th hour, 16 of them are between -1.54 and 2.06 TECU for 16th hour, 9 of them are between -0.39 and 0.91 TECU for 18th hour, 10 of them are between -0.88 and 0.32 TECU for 20th hour and 11 of them are between -1.52 and 0.58 TECU for 22th hour.

At the DIDI station, 9 of the 20 normalised TEC values are between -0.52 and 0.48 TECU for 0th hour, 11 of them are between -0.32 and 0.78 TECU for 2nd hour, 18 of them are between -1.17 and 1.17 TECU for 4th hour, 11 of them are between -0.68 and 0.72 TECU for 6th hour, 10 of them are between -1.04 and 0.74 TECU for 8th hour, 11 of them are between -1.60 and 0.40 TECU for 10th hour, 16 of them are between -1.22 and 1.57 TECU for 12th hour, 16 of them are between -1.68 and 1.92 TECU for 14th hour, 14 of them are between -1.50 and 1.51 TECU for 16th hour, 8 of them are between -0.35 and 0.95 TECU for 18th hour, 9 of them are between -0.88 and 0.22 TECU for 20th hour and 9 of them are between -0.51 and 0.59 TECU for 22th hour.

At the DNZ1 station, 9 of the 20 normalised TEC values are between -0.46 and 0.54 TECU for 0th hour, 11 of them are between -0.39 and 0.61 TECU for 2nd hour, 17 of them are between -1.20 and 1.20 TECU for 4th hour, 10 of them are between -0.71 and 0.69 TECU for 6th hour, 10 of them are between -1.12 and 0.68 TECU for 8th hour, 12 of them are between -1.56 and 0.44 TECU for 10th hour, 13 of them are between -1.22 and 1.43 TECU for 12th hour, 14 of them are

between -1.68 and 1.24 TECU for 14th hour, 9 of them are between -1.35 and 0.45 TECU for 16th hour, 8 of them are between -0.40 and 0.90 TECU for 18th hour, 9 of them are between -0.87 and 0.23 TECU for 20th hour and 9 of them are between -0.45 and 0.75 TECU for 22th hour.

At the IZMI station, 9 of the 20 normalised TEC values are between -0.34 and 0.76 TECU for 0th hour, 11 of them are between -0.21 and 0.89 TECU for 2nd hour, 16 of them are between -1.20 and 1.23 TECU for 4th hour, 11 of them are between -0.73 and 0.67 TECU for 6th hour, 10 of them are between -1.13 and 0.67 TECU for 8th hour, 12 of them are between -1.61 and 0.29 TECU for 10th hour, 15 of them are between -0.99 and 1.54 TECU for 12th hour, 16 of them are between -1.66 and 1.94 TECU for 14th hour, 9 of them are between -1.34 and 0.41 TECU for 16th hour, 12 of them are between -0.98 and 0.99 TECU for 18th hour, 10 of them are between -0.74 and 0.36 TECU for 20th hour and 9 of them are between -0.39 and 0.81 TECU for 22th hour.

At the MUG1 station, 9 of the 20 normalised TEC values are between -0.51 and 0.49 TECU for 0th hour, 10 of them are between -0.43 and 0.57 TECU for 2nd hour, 17 of them are between -1.14 and 1.14 TECU for 4th hour, 10 of them are between -0.70 and 0.70 TECU for 6th hour, 10 of them are between -1.06 and 0.74 TECU for 8th hour, 11 of them are between -1.61 and 0.39 TECU for 10th hour, 13 of them are between -0.99 and 1.56 TECU for 12th hour, 13 of them are between -1.68 and 1.28 TECU for 14th hour, 9 of them are between -1.42 and 0.38 TECU for 16th hour, 9 of them are between -0.33 and 0.97 TECU for 18th hour, 9 of them are between -0.94 and 0.16 TECU for 20th hour and 12 of them are between -0.54 and 0.56 TECU for 22th hour.

At the KIKA station, 9 of the 20 normalised TEC values are between -0.29 and 0.81 TECU for 0th hour, 16 of them are between -0.86 and 0.98 TECU for 2nd hour, 17 of them are between -1.35 and 1.25 TECU for 4th hour, 11 of them are between -0.69 and 0.81 TECU for 6th hour, 10 of them are between -1.18 and 0.62 TECU for 8th hour, 12 of them are between -1.52 and 0.38 TECU for 10th hour, 17 of them are between -1.40 and 1.40 TECU for 12th hour, 15 of them are between -1.74 and 1.86 TECU for 14th hour, 10 of them are between -1.29 and 0.51 TECU for 16th hour, 8 of them are between -0.35 and 0.95 TECU for 18th hour, 10 of them are between -0.61 and 0.49 TECU for 20th hour and 10 of them are between -0.35 and 2.05 TECU for 22th hour.

At the SALH station, 9 of the 20 normalised TEC values are between -0.339 and 0.77 TECU for 0th hour, 11 of them are between -0.22 and 0.88 TECU for 2nd hour, 15 of them are between -0.64 and 1.21 TECU for 4th hour, 11 of them are between -0.72 and 0.68 TECU for 6th hour, 10 of them are between -1.13 and 0.67 TECU for 8th hour, 12 of them are between -1.58 and 0.32 TECU for 10th hour, 14 of them are between -1.99 and 1.52 TECU for 12th hour, 15 of them are between -1.77 and 1.83 TECU for 14th hour, 9 of them are between -1.33 and 0.47 TECU for 16th hour, 13 of them are between -0.96 and 0.93 TECU for 18th hour, 11 of them are between -0.73 and 0.39 TECU for 20th hour and 9 of them are between -0.37 and 0.83 TECU for 22th hour.

After the TEC values were normalised and found to be in normal distribution, the F_{test} was used. In the comparison, test value is as follows:

$$F_{test} = \frac{m_i^2}{m_j^2} \tag{4}$$

The F_{test} value is compared with $F_{table} = F_{f_1,f_2,1-\alpha}$. The bigger variance value has to be written at the numerator while the usage of Eq. 4 (Ghilani and Wolf, 2006). The F_{test} values obtained for consecutive days of each station are shown in Table 5.

When Tables 3 and 5 are examined together, the significant differences were determined on the days 294-295, 295-296, 296-297, 304-305, 305-306, 308-309, 309-310 and 310-311.

Table 5 - Statistical test values for RIM.

Stations	AYD1	AYVL	CESM	DATC	DIDI	DNZ1	IZMI	MUG1	KIKA	SALH
Day										
294-295	2.019*	2.071*	2.048*	2.128*	2.006*	1.993*	2.036*	2.143*	2.110*	1.965*
295-296	2.546*	2.032*	2.684*	2.374*	2.962*	2.124*	2.688*	2.435*	2.401*	2.769*
296-297	2.004*	2.018*	2.113*	1.997*	2.338*	1.696	2.115*	1.232	2.144*	2.088*
297-298	1.370	1.738	1.563	1.750	1.420	2.158*	1.575	2.018*	1.822	1.491
298-299	1.041	1.390	1.080	1.041	1.008	1.054	1.016	1.317	1.299	1.021
299-300	1.663	1.703	1.689	1.601	1.646	1.619	1.690	1.226	1.683	1.670
300-301	1.178	1.126	1.157	1.178	1.179	1.174	1.153	1.179	1.132	1.159
301-302	1.009	1.205	1.211	1.005	1.005	1.005	1.008	1.066	1.049	1.148
302-303	1.720	1.435	1.434	1.678	1.718	1.712	1.753	1.821	1.647	1.510
303-304	1.771	1.641	1.651	1.863	1.895	1.784	1.658	1.889	1.655	1.717
304-305	2.091*	2.182*	2.056*	2.049*	2.092*	2.080*	2.001*	2.076*	2.063*	2.026*
305-306	2.106*	2.083*	2.077*	2.070*	2.068*	2.005*	2.192*	2.025*	2.058*	2.039*
306-307	1.020	1.068	1.037	1.056	1.052	1.036	1.050	1.037	1.022	1.004
307-308	1.263	1.432	1.293	1.231	1.226	1.233	1.359	1.259	1.346	1.367
308-309	2.018*	2.474*	2.002*	2.085*	2.009*	2.012*	2.097*	2.093*	2.027*	2.128*
309-310	2.724*	2.013*	2.058*	2.747*	2.697*	2.246*	2.588*	2.491*	2.543*	2.625*
310-311	1.507	2.090*	2.140*	1.557	1.799	2.002*	2.058*	1.793	2.095*	2.032*
311-312	1.026	1.593	1.416	1.064	1.241	1.667	1.451	1.349	1.486	1.421
312-313	1.059	1.375	1.385	1.072	1.053	1.038	1.030	1.066	1.022	1.042
* significant difference										

After RIM-TEC values are obtained, to determine whether there is any TEC anomaly, lower bounder (*LB*) and upper bounder (*UB*) values are calculated as follows:

$$UB = M + 1.34\sigma \quad (5)$$

$$LB = M - 1.34\sigma \quad (6)$$

where M and σ represent the mean and standard deviation of TEC values in Eqs. 5 and 6, respectively. The RIM-TEC values are in normal distribution with mean value (m) and standard deviation (σ), and M, LB and UB values have been obtained with a confidence of 1.34σ and m (Klotz and Johnson, 1983). In determining which day is the anomaly day, if one-third of the TEC values of that day fall above the upper limit or below the lower limit, that day is expressed as the anomaly day (Liu *et al.*, 2009).

It is important to determine Vertical TEC (*VTEC*) values because earthquakes show both horizontal and vertical movements. After Slant TEC (*STEC*) is calculated, *VTEC* values for each day have been calculated with:

$$VTEC = STEC \times \cos\left(\arcsin\left(\frac{R\sin Z}{R+H}\right)\right) \quad (7)$$

here, *z* is the zenith angle for the satellite, *R* is radius of Earth, and *H* is the distance from the Earth's surface to the single layer.

3. Results and discussion

Anomaly values of CORS-TR stations used were determined with the help of Eqs. 5 and 6. The anomaly graphics are shown in Figs. 3 and 4.

In Figs. 3 and 4, red and green squares denote positive and negative anomalies respectively. When Fig. 3 is examined, it is seen that all stations have a positive anomaly on the 296th and 305th day of year 2020, and in addition to these, there is a positive change on the 297th day of year 2020 in the DNZ1 and MUG1 stations. This situation shows that there is a maximum anomaly 8 days before the 304th day of year 2020, which is the earthquake day, and this change continues in a positive way one day after the earthquake (black line in Figs. 3 and 4). On the other hand, the negative directional anomaly change is seen to occur in all stations 9 days before the earthquake day (295th day of year 2020). Also, Fig. 4 shows that there are only positive anomalies for CODE (Table 6). It can be thought that the anomaly changes occurring after the earthquake are due to the aftershocks induced by the earthquake (Table 7).

Table 6 - Days with positive and negative anomaly and anomaly values (TECU).

Day	**295**		**296**	**297**		**298**	**299**	**300**	**302**	**305**		**309**	**311**
Station	**RIM$^-$**	**CODE$^+$**	**RIM$^+$**	**RIM$^+$**	**CODE$^+$**	**CODE$^+$**	**CODE$^+$**	**CODE$^+$**	**CODE$^+$**	**RIM$^+$**	**CODE$^+$**	**RIM$^-$**	**RIM$^-$**
AYD1	0.615	2.172	1.120	-	-	2.507	1.281	1.251	0.588	0.542	1.405	0.509	-
AYVL	0.477	2.028	1.373	-	-	2.152	1.544	1.444	-	0.669	1.444	0.437	0.886
CESM	0.573	2.153	1.264	-	0.589	2.412	1.472	1.406	0.460	0.534	1.373	0.427	0.796
DATC	0.722	2.235	0.928	-	0.826	2.720	1.147	1.174	0.633	0.556	1.236	0.551	-
DIDI	0.676	2.225	1.045	-	0.732	2.590	1.282	1.264	0.547	0.529	1.336	0.513	-
DNZ1	0.603	2.149	1.077	0.313	0.688	2.675	1.152	1.141	0.739	0.569	1.445	0.582	0.699
IZMI	0.573	2.127	1.216	-	0.583	2.332	1.413	1.353	0.521	0.55	1.410	0.464	0.766
MUG1	0.669	2.209	0.989	0.348	0.766	2.651	1.154	1.159	0.691	0.553	1.349	0.56	-
KIKA	0.506	2.026	1.296	-	0.472	2.313	1.426	1.346	0.612	0.643	1.478	0.47	0.819
SALH	0.559	2.090	1.204	-	0.577	2.460	1.319	1.269	0.602	0.574	1.460	0.486	0.75

It can be seen that the RMSEs obtained from the CODE-TEC values vary in the range of ±2.857 - ±4.080, ±2.645 - ±3.922, ±2.798 - ±4.099, ±2.999 - ±4.245, ±2.927 - ±4.185, ±2.858 - ±4.018, ±2.780 - ±4.040, ±2.934 - ±4.138, 2.674 - ±3.895, ±2.763 - ±3.964 for AYD1, AYVL, CESM, DATC, DIDI, DNZ1, IZMI, MUG1, KIKA, SALH, respectively (Table 5). It can be observed, also, that the RMSEs obtained from RIM-TEC vary in the range of ±2.109 - ±3.955, ±2.130 - ±3.972, ±2.232 - ±3.966, ±2.233 - ±3.982, ±2.161 - ±3.886, ±2.327 - ±3.975, ±2.091 - ±3.911, ±2.292 - ±3.949, ±2.061 - ±3.886, ±2.091 - ±3.870 for AYD1, AYVL, CESM, DATC, DIDI, DNZ1, IZMI, MUG1, KIKA,SALH, respectively (Table 4). When the RMSEs obtained from both CODE-TEC and RIM-TEC are compared, it can be noted that the RMSEs obtained from RIM-TEC are better than the RMSEs from CODE-TEC. If the RMSEs are bigger, the probability of being in agreement with each other increases in the statistical comparison (Ghilani and Wolf, 2006). In addition, it can be seen in Table 6 that the CODE-TEC values have a one-way anomaly. It can be seen, as well, that the

fact that RMSE values are big and have only positive anomaly causes the calculated RMSEs to be statistically equal with each other on consecutive days. We, then, think that the F_{test} values, calculated from the CODE-TEC, vary between 1.854 and 1.000, and the RMSEs are statistically equal with each other due to the reasons mentioned above.

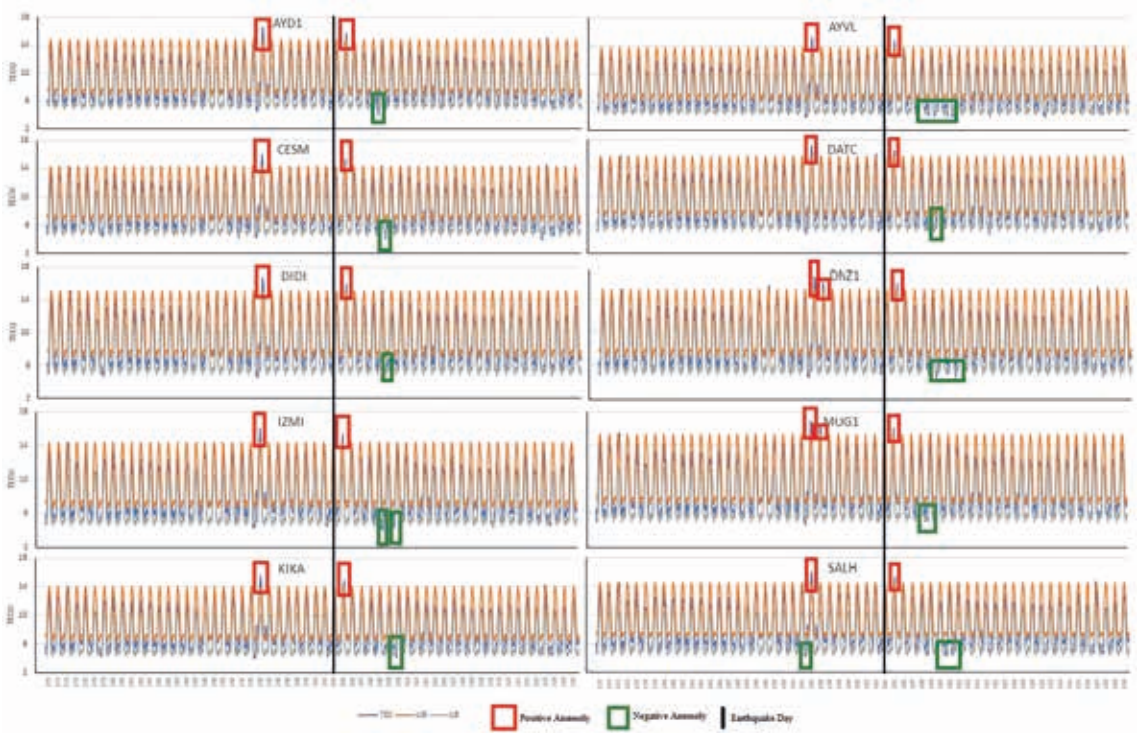

Fig. 3 - *UB*, *LB* and TEC values for RIM.

Examining the anomalies reported Table 6, it can be seen that the anomalies calculated from CODE-TEC are positive, and the anomalies calculated from RIM-TEC are positive or negative depending on earthquake and aftershocks. The anomalies calculated from CODE-TEC are in the range of 0.460 - 2.675 TECU. When the anomalies calculated from RIM-TEC are examined, it can be observed that negative anomalies are in the range of 0.477 - 0.886 TECU, and positive anomalies are in the range of 0.313 - 1.373 TECU. In addition, when Tables 3, 4, and 5 are examined together, it is clearly seen that the RMSE values are not statistically equal with each other on consecutive days when different anomalies occur. Moreover, it can be noted in Table 6 that the maximum anomaly values calculated from RIM-TEC remained smaller than the anomaly values calculated from CODE-TEC on the 295th, 297th, and 305th day of year 2020, as absolute values. Also, in Tables 3 and 4, it can be seen that the RMSE values calculated from RIM-TEC were better than RMSE values calculated with CODE-TEC. This proves that the RMSE values calculated from RIM-TEC are more precise. The RMSE of IGS IONEX TEC values were defined in the range of 2-8 TECU (Hernández-Pajares *et al.*, 2009; Zhang and Zhao, 2018). The results in Tables 3 and 4 show that the calculated RMSEs of RIM-TEC values are within the acceptable range and, hence, can be considered reliable.

When Table 7 is examined, it can be seen that, after the Seferihisar-Izmir earthquake, 420

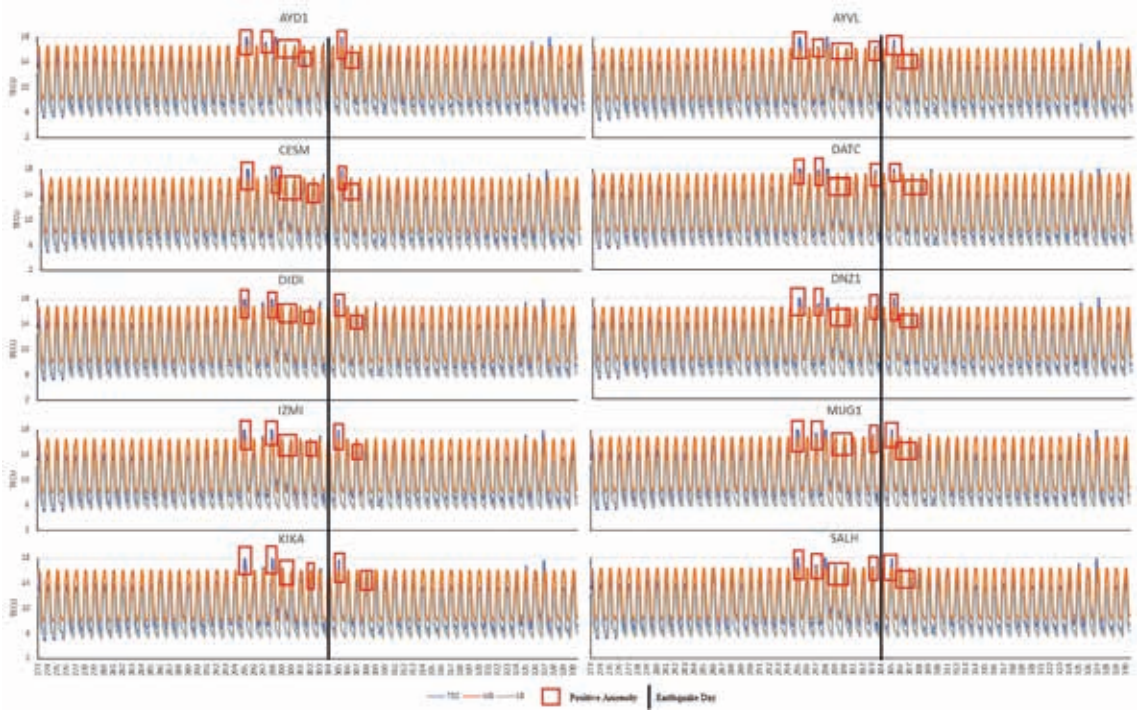

Fig. 4 - *UB*, *LB* and TEC values for CODE.

Table 7 - The number of aftershocks (URL 7).

Day of year	Date	*Mw*			
		3.0 - 3.9	**4.0 - 4.9**	**5.0 - 5.9**	**6.0 - 6.9**
304	30.10.2020	131	28	1	1
305	31.10.2020	92	17	1	
306	1.11.2020	45	5		
307	2.11.2020	31	2		
308	3.11.2020	14	1		
309	4.11.2020	13	1		
310	5.11.2020	14			
311	6.11.2020	12	1		
312	7.11.2020	7			
313	8.11.2020	4			
Total		363	55	2	1

aftershocks occurred: 363 are in the range $3.0 \leq M_w \leq 3.9$, 55 in the range $4.0 \leq M_w \leq 4.9$, and the remaining ones are between M_w 5.0 and 5.9. Furthermore, 110 of these aftershocks occurred one day after the earthquake (305th day of year 2020).

Comparative graphics of CODE-TEC and RIM-TEC values of days with positive TEC anomaly are given in Figs. 5 to 7.

When Figs. 3 to 7 are examined together, it can be seen that there is a substantial similarity between RIM-TEC values and CODE-TEC values, and RIM-TEC and CODE-TEC values increase up

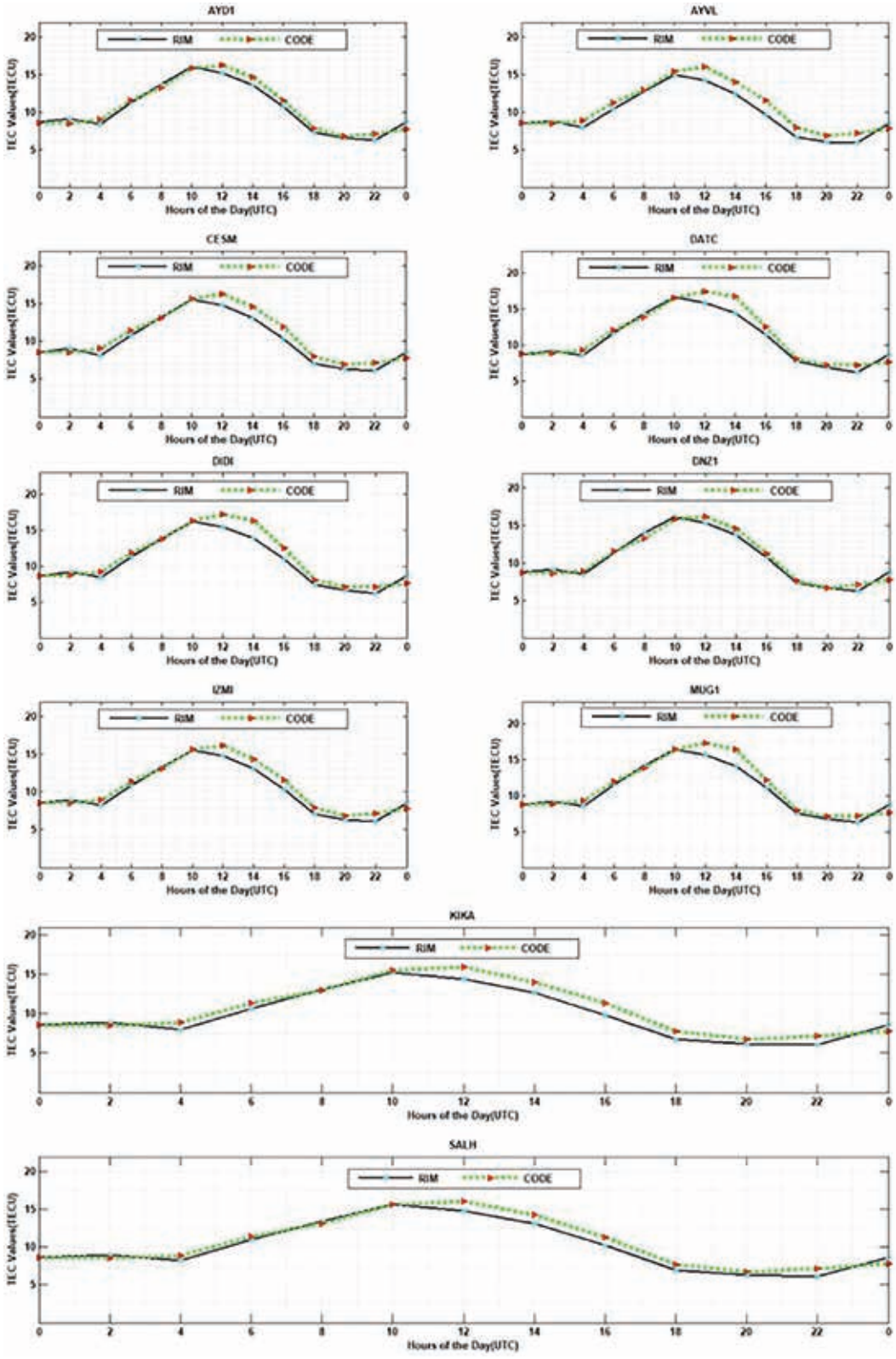

Fig. 5 - TEC values for the 296th day for year 2020.

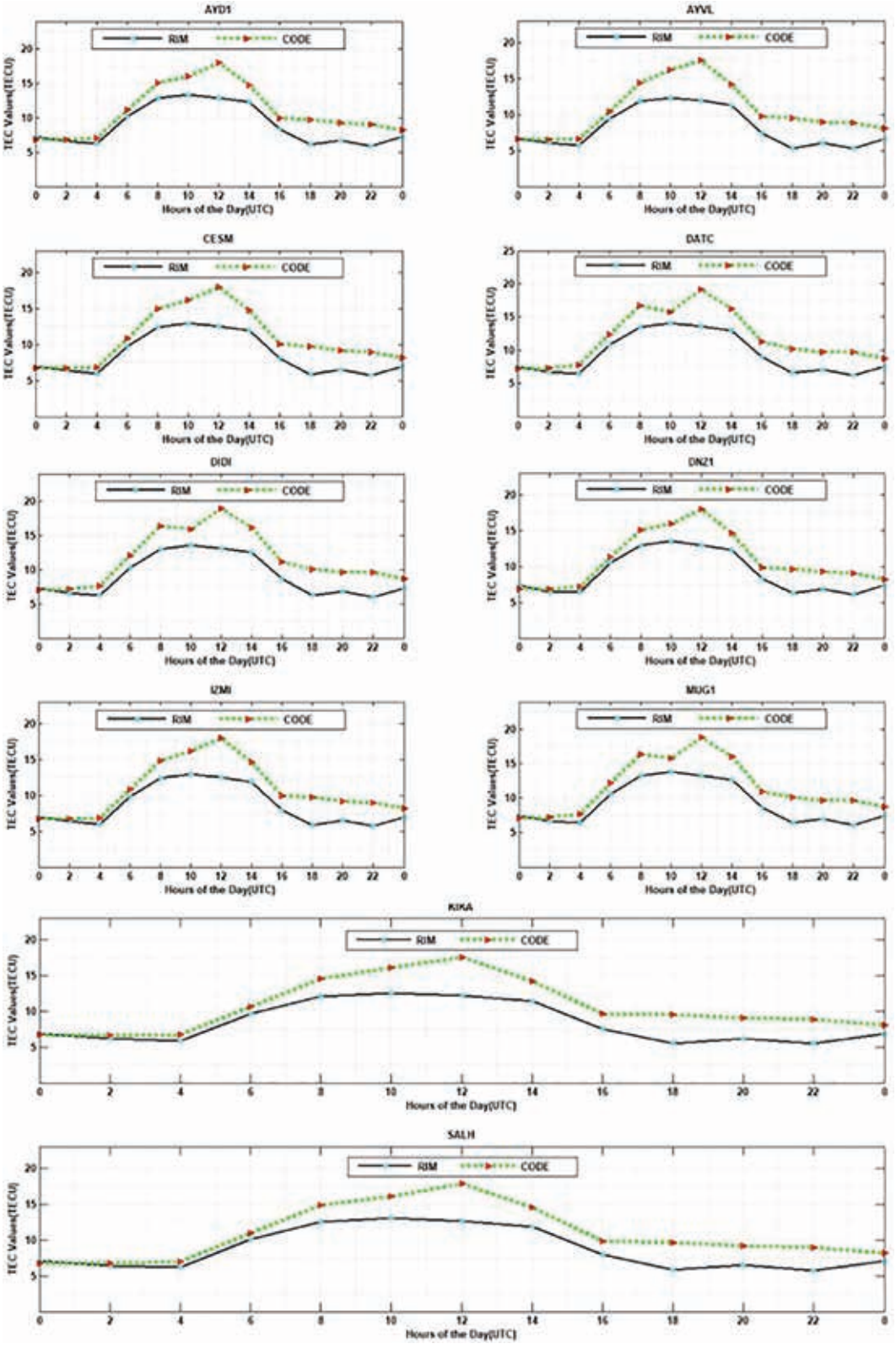

Fig. 6 - TEC values for the 304th day for year 2020.

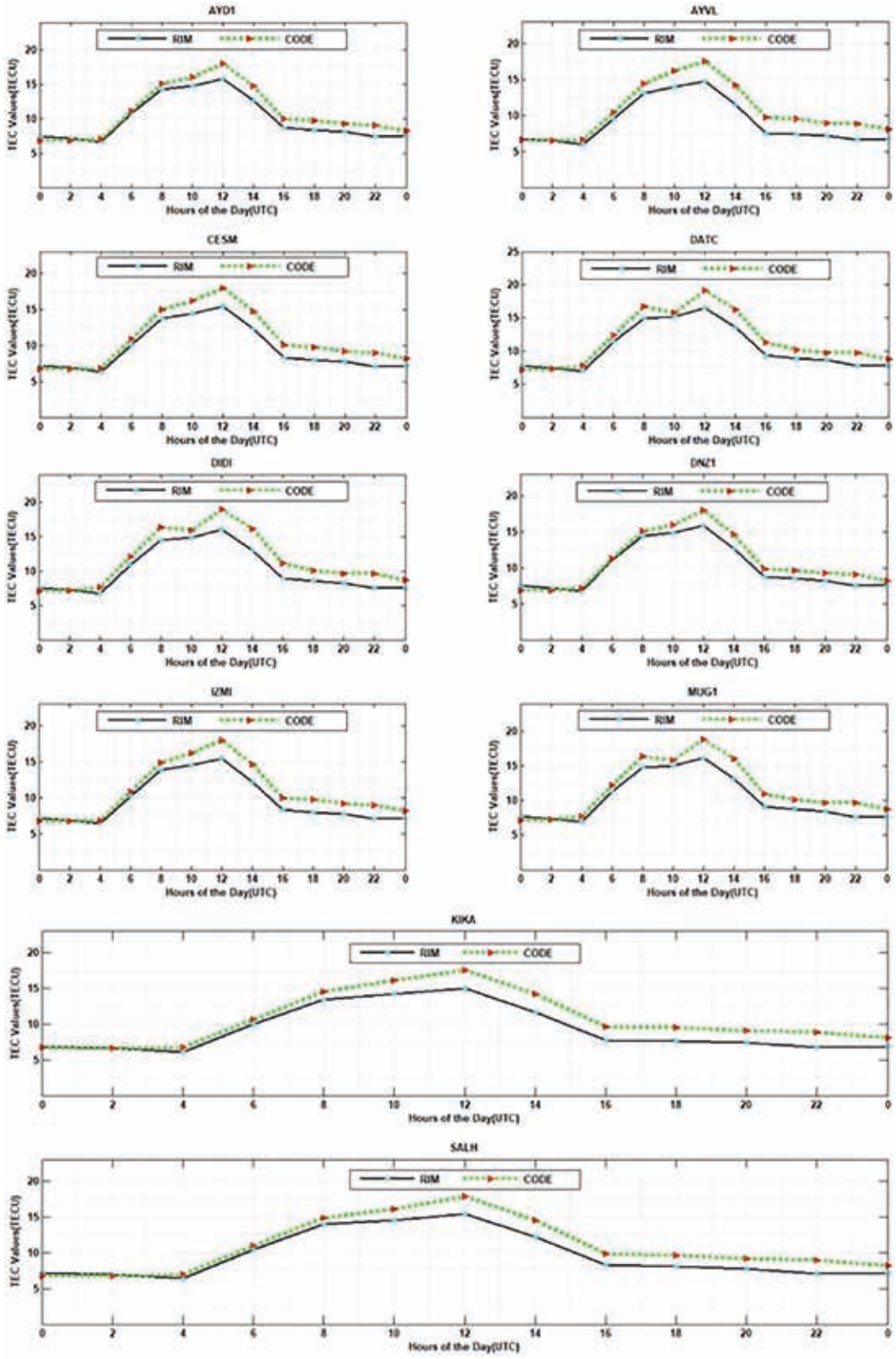

Fig. 7 - TEC values for the 305th day for year 2020.

to noon and, then, decrease. Also, it can be seen that RIM-TEC values are considerably lower than CODE-TEC values on other days except for the 296th day of 2020, and RIM-TEC values approach and sometimes exceed CODE-TEC values on the 296th day of 2020. It is clearly seen that there are some differences between CODE-TEC values and RIM-TEC values. Global TEC maps are produced daily by CODE using ~300 IGS GNSS stations. While producing global TEC maps, one (ANKR station) of 6 GNSS stations in Turkey is used. The difference between global TEC and regional TEC values is thought to be due to the fact that IGS stations are not used in Turkey. The positive anomaly on the 305th day of year 2020 after the earthquake is thought to be caused by the aftershocks following the earthquake (Table 7).

After the STEC values were determined, VTEC values were calculated by Eq. 7. Maximum VTEC values for positive anomalies are given in Fig. 8.

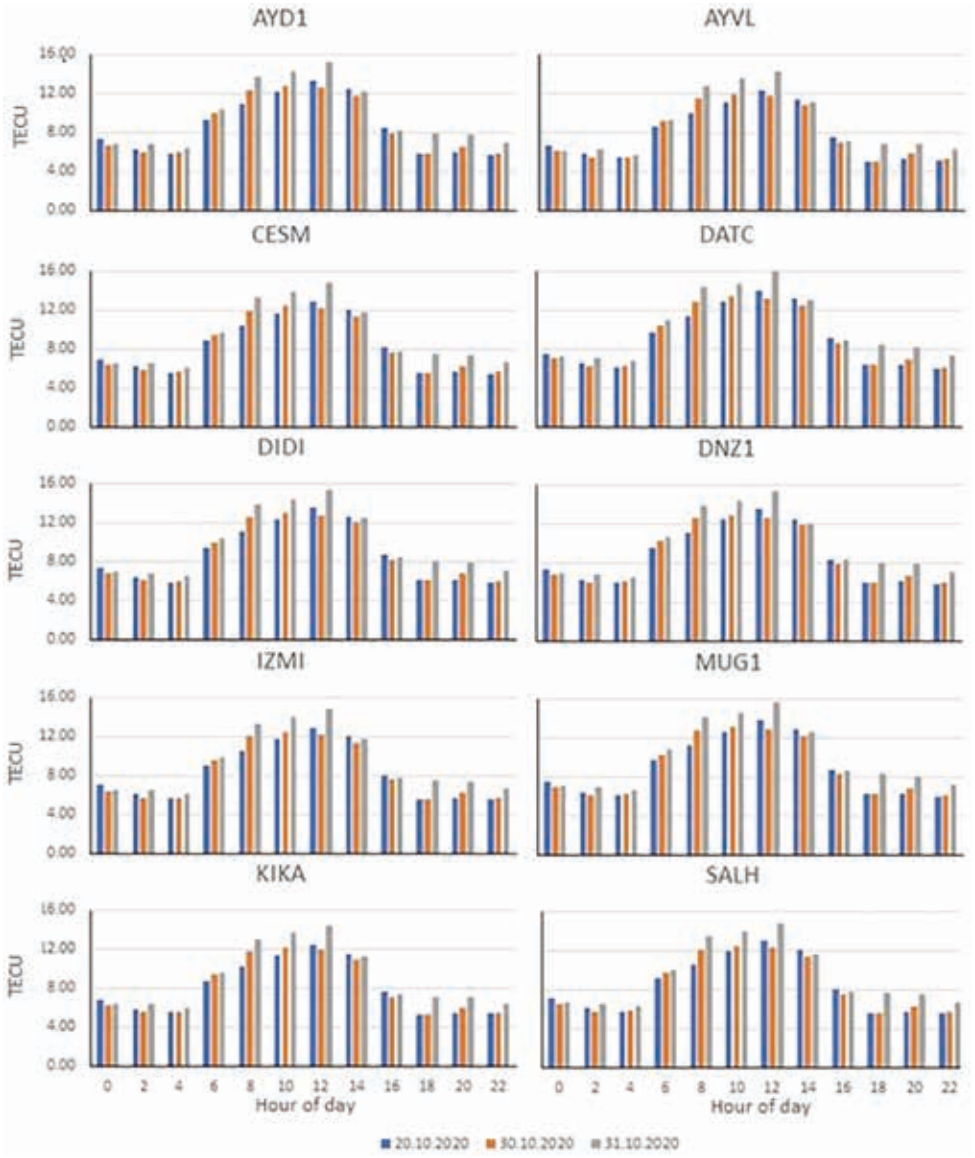

Fig. 8 - VTEC values for RIM.

It may be argued from Fig. 8 that the highest VTEC values occurred 8 days before the earthquake (296th day of year 2020). Also, it is observed that there is a decrease in VTEC values per each day after the earthquake, and, then, VTEC values increase again with the effect of aftershocks. In Fig. 8, blue, orange, and grey bars denote the days 22, 30, and 31 October 2020, respectively.

4. Conclusions

The ionosphere layer varies depending on factors such as solar activity, seasonal change, day and night, location, geomagnetic activity, and earthquakes. Although the change occurring in this layer is mostly caused by the Sun, the other effects mentioned should be considered for ionosphere modelling. Studies carried out in order to minimise loss of life and property caused by earthquakes have recently become more popular among scientists. Today, studies to determine any ionospheric anomalies are increasing day by day due to TEC changes in the ionosphere that occurred before earthquakes. GNSS measurements are used when determining the TEC changes, but the geomagnetic activities affect these measurements. Therefore, it is important to differentiate TEC changes caused by earthquakes and by geomagnetic activities.

If there is no significant geomagnetic activity, TEC changes can be related to earthquakes. In this study, the effect of the M_W 6.6 earthquake, that occurred in the north of Samos Island in the Aegean Sea according to AFAD, was investigated for TEC changes. Bernese v5.2 Scientific GNSS software was used to calculate RIM-TEC values. RIM-TEC values obtained by processing GNSS data were compared with CODE-TEC from Global TEC maps. The comparison shows that RIM-TEC values are similar to CODE-TEC, in that they increase almost every day from Coordinated Universal Time (UTC) 0:00 to UTC 12:00 and, then, decrease. On 22 October 2020, only eight days before the earthquake, it can be seen that the TEC changes differed from the normal course of changes and exceeded the daily expected change.

It can be observed that the RMSE values of RIM-TEC varied between ±2.061 - ±3.977 TECU, and the RMSE values of CODE-TEC varied between ±2.645 and ±4.245 TECU in selected days. In addition, it is clearly seen that the RMSE values are not statistically equal with each other on consecutive days when different anomalies occur. Also, it can be seen that the maximum anomaly values calculated from RIM-TEC remained lower than the anomaly values calculated from CODE-TEC and the RMSE values calculated with RIM-TEC were better than the RMSE values calculated with CODE-TEC. The RMSE of IGS IONEX TEC values were defined in the range of 2-8 TECU. The results show that the calculated RMSE values are within an acceptable range and, hence, can be considered reliable. By using the F-test, it was compared whether consecutive days had statistically significant differences with each other. The comparison shows that the days without any TEC anomalies were in agreement with each other, but the days with positive/negative anomalies were inconsistent with the other days.

When the VTEC values are examined, it can be seen that the highest VTEC values occurred eight days before the earthquake. It was determined that the VTEC values returned to normal towards the earthquake day and increased again with energy released before the aftershocks that occurred after the earthquake.

When RIM-TEC and CODE-TEC values are compared in the absence of an earthquake, it can be noted that CODE-TEC values are higher than RIM-TEC values. Global TEC maps are created using IGS stations spread all over the world. TEC values (CODE-TEC), calculated for the desired region by using global TEC maps, are determined by interpolation. Regional TEC values (RIM-TEC) are

calculated by the TEC maps created as a result of the analysis of the data of the GNSS stations in the desired area. The reason why the TEC values calculated from the Global TEC maps are higher than the regionally calculated TEC values is due to the interpolation performed from longer distances (Basciftci, 2017; Basciftci *et al.*, 2017, 2018). It was determined that the difference between the TEC values, except for the 296th and 305th day, ranged from 0.63 to 3.31 TECU. However, it was calculated that the difference between CODE-TEC and RIM-TEC values changed between 0.11 and 0.98 TECU 8 days before the earthquake (296th day of year 2020) and on the day when intense aftershocks occurred (305th day of 2020). In the selected days, the differences of the RMSE values, which are calculated with both CODE-TEC and RIM-TEC, range between ±0.001 to ±1.570 TECU. The maximum difference between RMSE values was determined on the 298th day when CODE-TEC values had positive anomaly when all stations were considered.

In terms of anomalies, CODE-TEC values were found to have positive anomaly before/after the earthquake. When the CODE-TEC values, which belong to ~30 days before the earthquake, were examined, it was seen that the positive change begins 8 days before earthquake in the anomalies calculated with the CODE-TEC values. The chance of detecting positive anomalies in the ionospheric TEC seems not to be a function of time and there is no clear tendency for ionospheric positive anomalies. The statements are supported by previous papers (Liu *et al.*, 2004, 2006, 2010; Le *et al.*, 2011). Besides, Le *et al.* (2011) also depicted the relationship of ionospheric anomalies and earthquakes with M > 6.0 during 2002-2010 in the whole world. Furthermore, they also showed a high occurrence rate of positive anomalies within 1 to 21 days.

When the RIM-TEC values of ~30 days before the earthquake are examined, it is seen that the positive and negative changes in the anomalies calculated with the RIM-TEC values also begin 8 days before the earthquake. Our previous study (Bulbul and Basciftci, 2021) and Zhu *et al.* (2014) support this. In this case, the fact that positive and negative changes occurred 8 days before the earthquake suggests that the possible energy released before the main shocks has an effect on RIM-TEC values.

REFERENCES

Alcay S. and Gungor M.; 2020: *Investigation of ionospheric TEC anomalies caused by space weather conditions*. Astrophys. Space Sci., 365, 150, doi: 10.1007/s10509-020-03862-x.

Aquino M., Waugh S., Dodson A., Moore T. and Skone S.; 2001: *GPS based ionosphere scintillation monitoring*. In: Proc. Space Weather Workshop: Looking Towards a Future Europen Space Weather Programme, ESTEC, Noordwijk, The Netherlands, 4 pp.

Arslan N.; 2004: *Investigation of the effects of the ionospheric total electron content variations on the coordinates using GPS*. Ph.D. Thesis, Yildiz Technical University, Istanbul, Turkey, (in Turkish).

Bartels J.; 1938: *Potsdamer erdmagnetische Kennziffern. 1. Mitteilung.* Zeitschrift für Geophysik, 14, 68-78, doi: 10.23689/fidgeo-3165.

Bartels J., Heck N.H. and Johnston H.F.; 1939: *The three-hour-range index measuring geomagnetic activity*. J. Geophys. Res., 44, 411-454, doi: 10.1029/TE044i004p00411.

Basciftci F.; 2017: *The creation of ionosphere model using GNSS data and its comparison with global models*. Ph.D. Thesis, Selçuk University, Konya, Turkey, 296 pp. (in Turkish).

Basciftci, F., Inal C., Yildirim O. and Bulbul S.; 2017: *Determining regional ionospheric model and comparing with global models*. Geodetski Vestnik, 61, 427-440, doi: 10.15292/geodetski-vestnik.2017.03.427-440.

Basciftci F., Inal C., Yildirim O. and Bulbul S.; 2018: *Comparison of regional and global TEC values: Turkey model*. Int. J. Eng. Geosci., 3, 61-72, doi: 10.26833/ijeg.382604.

Bhattacharya S., Dubey S., Tiwari R., Purohit P.K. and Gwal A.K.; 2008: *Effect of magnetic activity on ionospheric time delay at low latitude*. J. Astrophys. Astron., 29, 269-274, doi: 10.1007/s12036-008-0035-9.

Bulbul S. and Basciftci F.; 2021: *TEC anomalies observed before and after Sivrice-Elaziğ earthquake (24 January 2020, Mw: 6.8)*. Arabian J. Geosci., 14, 1077, doi: 10.1007/s12517-021-07426-3.

Eisenbeis J. and Occhipinti G.; 2021: *The TEC enhancement before seismic events is an artifact*. J. Geophys. Res. A: Space Phys., 126, e28733, 11 pp., doi: 10.1029/2020JA028733.

Elghazouly A.A., Doma M.I. and Sedeek A.A.; 2019: *Estimating satellite and receiver differential code bias using a relative Global Positioning System network*. Ann. Geophys., 37, 1039-1047, doi: 10.5194/angeo-37-1039-2019.

Elsayed A., Sedeek A., Doma M. and Rabah M.; 2018: *Vertical ionospheric delay estimation for single-receiver operation.* J. Appl. Geod., 13, 81-91, doi: 10.1515/jag-2018-0041.

Fleming J.A., Harradon H.D. and Joyce J.W.; 1939: *Seventh General Assembly of the Association of Terrestrial Magnetism and Electricity, Washington, D.C.* Terr. Magn. Atmos. Electr., 44, 471-479, doi: 10.1029/TE044i004p00471.

Fuying Z., Yun W. and Ningbo F.; 2011: *Application of Kalman filter in detecting pre-earthquake ionospheric TEC anomaly*. Geod. Geodyn., 2, 43-47, doi: 10.3724/SP.J.1246.2011.00043.1.

Ghilani C.D. and Wolf P.R.; 2006: *Adjustment computations: spatial data analysis, 4th ed.* John Wiley and Sons Inc., Hoboken, NJ, USA, 634 pp., doi: 10.1002/9780470121498.

Hernández-Pajares M., Juan J.M., Sanz J., Orus R., Garcia-Rigo A., Feltens J., Komjathy A., Schaer S.C. and Krankowski A.; 2009: *The IGS VTEC maps: a reliable source of ionospheric information since 1998*. J. Geod., 83, 263-275, doi: 10.1007/s00190-008-0266-1.

Hofmann-Wellenhof B., Lichtenegger H. and Wasle E.; 2008: *GNSS - Global Navigation Satellite Systems, GPS, GLONASS, Galileo & more*. Springer, Wien, Austria, 545 pp.

Hunsucker R.D. and Hargreaves J.K.; 2003: *The high-latitude ionosphere and its effects on radio propagation*. Cambridge University Press, Cambridge, UK, 636 pp.

Jakowski N., Wehrenpfenning A., Heise S., Schluter S. and Noack T.; 2001: *Space weather effects in the ionosphere and their impect on positioning*. In: Proc. Space Weather Workshop: Looking Towards a Future Europen Space Weather Programme, ESTEC, Noordwijk, The Netherlands, 7 pp.

Karia S.P., Pathak K.N., Yadav K.S., Chaudhary N.P., Patel N.C. and Jana R.; 2014: *Modification in atmospheric refractivity and GPS based TEC as earthquake precursors*. Positioning, 5, 46-52, doi: 10.4236/pos.2014.52006.

Ke F., Wang J., Tu M., Wang X., Wang X., Zhao X. and Deng J.; 2018: *Enhancing reliability of seismo-ionospheric anomaly detection with the linear correlation between total electron content and the solar activity index F10.7: Nepal earthquake 2015*. J. Geodyn., 121, 88-95, doi: 10.1016/j.jog.2018.07.001.

Klobuchar J.A.; 1991: *Ionospheric effects on GPS*. GPS World, 2, 48-51.

Klotz S. and Johnson N.L.; 1983: *Encyclopedia of statistical sciences*. John Wiley and Sons, Hoboken, NJ, USA, 672 pp.

Le H., Liu J.Y. and Liu L.; 2011: *A statistical analysis of ionospheric anomalies before 736 M6.0+ earthquakes during 2002-2010*. J. Geophys. Res. Atmos., 116, A02303, doi: 10.1029/2010JA015781.

Liu J.Y., Chuo Y.J., Shan S.J., Tsai Y.B., Chen Y.I., Pulinets S.A. and Yu S.B.; 2004: *Pre-earthquake ionospheric anomalies registered by continuous GPS TEC measurements.* Ann. Geophys., 22, 1585-1593, doi: 10.5194/angeo-22-1585-2004.

Liu J.Y., Chen Y.I., Chuo Y.J. and Chen C.S.; 2006: *A statistical investigation of preearthquake ionospheric anomaly*. J. Geophys. Res., 111, A05304, doi: 10.1029/2005JA011333.

Liu J.Y., Chen Y.I., Chen C.H., Liu C.Y., Chen C.Y., Nishihashi M., Li J.Z., Xia Y.Q., Oyama K.I., Hattori K. and Lin C.H.; 2009: *Seismoionospheric GPS total electron content anomalies observed before the 12 May 2008 M(w)7.9 Wenchuan earthquake*. J. Geophys. Res. Space Phys., 114, A04320, doi: 10.1029/2008JA013698.

Liu J.Y., Chen Y.I., Chen C.H. and Hattori K.; 2010: *Temporal and spatial precursors in the ionospheric global positioning system (GPS) total electron content observed before the 26 December 2004 M9.3 Sumatra-Andaman earthquake*. J. Geophys. Res., 115, A09312, doi: 10.1029/2010JA015313.

Loewe C.A. and Prölss G.W.; 1997: *Classification and mean behavior ofmagnetic storms*. J. Geophys. Res., 102, 14209, doi: 10.1029/96JA04020.

Mosna Z., Sauli P. and Santolik O.; 2007: *Preparation of a database for the study of scaling phenomena in the ionosphere*. In: Proc. 16th Annual Conference of Doctoral Students - WDS 2007, Prague, Czechia, Part II, pp. 86-92.

Nishino M., Nozawa S. and Holtet J.A.; 1998: *Daytime ionospheric absorption features in the polar cap associated with poleward drifting F-region plasma patches.* Earth Planets Space, 50, 107-117, doi: 10.1186/BF03352092.

Oikonomou C., Haralambous H., Pulinets S., Khadka A., Paudel S.R., Barta V., Muslim B., Kourtidis K., Karagioras A. and Inyurt S.; 2021: *Investigation of pre-earthquake ionospheric and atmospheric disturbances for three large earthquakes in Mexico.* Geosci., 11, 16, doi: 10.3390/geosciences11010016.

Parkinson B.W. and Spilker J.J.; 1996: *Global positioning system: theory and applications*, *Vol. I*. American Institute of Aeronautics and Astronautics Inc., Washington, D.C., USA, 793 pp., doi: 10.2514/4.866388.

Ping J., Kono Y., Matsumoto K., Otsuka Y., Saito A., Shum C. and Kawano N.; 2002: *Regional ionosphere map over Japanese island.* Earth Planets Space, 54, e13-e16, doi: 10.1186/BF03352450.

Schaer S.; 1999: *Mapping and predicting the Earth's ionosphereusing the global positioning system.* Ph.D. Thesis in Philosophical Natural Sciences, Astronomical Institute, University of Berne, Berne, Switzerland, 228 pp.

Schaer S., Gurtner W. and Feltens J.; 1998: *IONEX: the ionosphere map exchange format, Version 1.* In: Proc. IGS Analysis Centers Workshop, ESOC, Darmstadt, Germany, pp. 233-247.

Sedeek A.; 2020: *Ionosphere delay remote sensing during geomagnetic storms over Egypt using GPS phase observations.* Arabian J. Geosci., 13, 811, doi: 10.1007/s12517-020-05817-6.

Sentürk E. and Cepni M.S.; 2018: *Ionospheric temporal variations over the region of Turkey: a study based on long-time TEC observations.* Acta Geod. Geophys., 53, 623-637, doi: 10.1007/s40328-018-0233-0.

Sentürk E., Inyurt S. and Sertcelik I.; 2020: *Ionospheric anomalies associated with the Mw 7.3 Iran-Iraq border earthquake and a moderate magnetic storm.* Ann. Geophys., 38, 1031-1043, doi: 10.5194/angeo-38-1031-2020.

Sharma K., Dabas R.S., Sarkar S.K., Das R.M., Ravindran S. and Gwal A.K.; 2010: *Anomalous enhancement of ionospheric F2 layer critical frequency and total electron content over low latitudes before three recent major earthquakes in China*. J. Geophys. Res., 115, 4-9, doi: 10.1029/2009JA014842.

Sickle J.V.; 2015: *GPS for land surveyors, 4th ed.* CRC Press, Boca Raton, FL, USA, 366 pp., doi: 10.1201/b18480.

Sidorov R., Soloviev A., Gvishiani A., Getmanov V., Mandea M., Petrukhin A., Yashin I. and Obraztsov A.; 2019: *A combined analysis of geomagnetic data and cosmic ray secondaries for the September 2017 space weather event studies.* Russ. J. Earth Sci., 19, 1-10, doi: 10. 2205/2019ES000671.

Skone S. and Cannon M.E.; 1999: *Ionospheric effects on differential GPS applications during auroral substorm activity.* ISPRS J. Photogramm. Remote Sens., 54, 279-288, doi: 10.1016/S0924-2716(99)00017-9.

Stewart P.J. and Langley R.B.; 1998: *Ionospheric modelling for WADGPS at northern latitudes.* In: Proc. 11th International Technical Meeting, ION GPS-98, Satellite Division of the Institute of Navigation, Nashville, TN, USA, pp. 757-765.

Tariq M.A., Shah M., Hernández-Pajares M. and Iqbal T.; 2019: *Pre-earthquake ionospheric anomalies before three major earthquakes by GPS-TEC and GIM-TEC data during 2015-2017.* Adv. Space Res., 63, 2088-2099, doi: 10.1016/j.asr.2018.12.028.

Teunissen P.J.G. and Kleusberg A.; 1998: *GPS for Geodesy, 2ed.* Springer, Berlin, Germany, 664 pp.

Thomas J.N., Huard J. and Masci F.; 2017: *A statistical study of global ionospheric map total electron content changes prior to occurrences of M ≥ 6.0 earthquakes during 2000-2014.* J. Geophys. Res. A: Space Phys., 122, 2151-2161, doi: 10.1002/2016JA023652.

Ulukavak M. and Yalcinkaya M.; 2014: *The relationship between Total Electron Content (TEC) valuesand earthquake*. Gümüşhane Univ. J. Sci. Technol. Inst., 4, 107-116, <dergipark.org.tr/tr/pub/gumusfenbil/article/98633>.

Ulukavak M. and Yalcinkaya M.; 2017: *Precursor analysis of ionospheric GPS-TEC variations before the 2010 M7.2 Baja California earthquake.* Geomatics, Nat. Hazard Risk, 8, 295-308, doi: 10.1080/19475705.2016.1208684.

Wild U.; 1994: *Ionosphere and geodetic satellite systems: permanent GPS tracking data for modeling and monitoring*. Geod.-Geophys. Arb. Schweiz, Vol. 48, 155 pp.

Ya'acob N., Abdullah M. and Ismail M.; 2010: *GPS Total Electron Content (TEC) prediction at ionosphere layer over the equatorial region.* In: Bouras C.J. (ed), Trends in Telecommunications Technologies, London, UK, pp. 485-508, doi: 10.5772/8474.

Yildirim O., Inyurt S. and Mekik C.; 2016: *Review of variations in Mw < 7 earthquake motions on position and TEC (Mw = 6.5 Aegean Sea earthquake sample).* Nat. Hazards Earth Syst. Sci., 16, 543-557, doi: 10.5194/nhess-16-543-2016.

Zhang Q. and Zhao Q.; 2018: *Global ionosphere mapping and differential code bias estimation during low and high solar activity periods with GIMAS software.* Remote Sens., 10, 705, doi: 10.3390/rs10050705.

Zhu F., Zhou Y., Lin J. and Su F.; 2014: *A statistical study on the temporal distribution of ionospheric TEC anomalies prior to M7.0+ earthquakes during 2003-2012.* Astrophys. Space Sci., 350, 449-457, doi: 10.1007/s10509-014-1777-2.

Zolesi B. and Cander L.R.; 2014: *Ionospheric prediction and forecasting.* Springer Verlag, Berlin-Heidelberg, Germany, 252 pp., doi: 10.1007/978-3-642-38430-1.

URL 1: *NOAA space weather scales.* <www.swpc.noaa.gov/noaa-scales-explanation> (last access: 01.09.2021).

URL 2: *Space weather Canada, solar radio flux - plot of monthly averages.* <www.spaceweather.gc.ca/forecast-prevision/solar-solaire/solarflux/sx-6-mavg-en.php> (last access: 03.03.2021).

URL 3: *AFAD, 30 October 2020 Aegean Sea, Seferihisar (Izmir) offshore (17.26 km) preliminary evaluation report on Mw 6.6 earthquake.* <deprem.afad.gov.tr/downloadDocument?id=2064> (last access: 05.03.2021).

URL 4: *Kandilli Observatory and Earthquake Research Institute, 30 October 2020 the Aegean Sea earthquake press release.* <www.koeri.boun.edu.tr/sismo/2/wp-content/uploads/2020/10/20201030_izmir_V1.pdf> (last access: 05.03.2021).

URL 5: <tr.wikipedia.org/wiki/2020_Ege_Denizi_depremi#cite_note-usgs-2> (last access: 30.08.2021).

URL 6: *Goddard Space Flight Center space physics data facility omni web.* <omniweb.gsfc.nasa.gov/form/dx1.html> (last access: 25.06.2021).

URL 7: *Kandilli Observatory and Earthquake Research Institute.* <udim.koeri.boun.edu.tr/zeqmap/hgmmap.asp> (last access: 05.07.2021).

Corresponding author: Fuat Basciftci
Vocational School of Technical Science, Karamanoğlu Mehmetbey University
Yanus Emre Campus, Karaman, Turkey
Phone: +90 5434455303, e-mail: ffanbasciftci@gmail.com